Multiple Defects Detection in Outer Race of Gearbox Ball Bearing Using Time Domain Statistical Parameters

A. Nabhan[a,c], M. Nouby[b], A.M. Sami[a] and M.O. Mousa[a]

[a]*Production and Design Dept., Faculty of Engg., Minia University, Minia, Egypt*
[b]*Mechanical Engg. Dept., Faculty of Engg., South Valley University, Qena, Egypt*
[c]*Corresponding Author, Email: a.nabhan@mu.edu.eg*

ABSTRACT:

Multiple defects are introduced on the outer race of vehicle gearboxes. The effect of the number of outer race defects in deep groove ball bearings are investigated using experimental and numerical methods. A three-dimensional model of the housing and outer race is developed using ABAQUS. Firstly, single defect located at 0° and two defects located at 0° and 67.5° are analyzed. Then the number of defects was increased to three and the locations of the local defects are 0°, 67.5° and 225°. Finally the model with four defects located on the outer race at the angular positions 0°, 67.5°, 225° and 270°, was investigated. The simulated data were also used to validate the experimental results.

CITATION:

A. Nabhan, M. Nouby, A.M. Sami and M.O. Mousa. 2016. Multiple Defects Detection in Outer Race of Gearbox Ball Bearing Using Time Domain Statistical Parameters, *Int. J. Vehicle Structures & Systems*, 8(3), 167-174. doi:10.4273/ijvss.8.3.09

1. Introduction

Vibration analysis is widely used in the condition monitoring applications since a defect produces successive impulses at every contact of defect and the rolling element, and the housing structure is forced to vibrate at its natural modes. The vibration pattern of a damaged bearing includes the low-frequency components related to the impacts and the high-frequency components. The structural information of the bearing structure is stored. A complex filter for Hilbert transformation is proposed to apply in the real-time vibration signal demodulation. A finite waveform interval of the proposed filter could be possibly applied in the vibration signal demodulation [1]. Experimental data were used to verify the validity of the developed algorithms. Both inner and outer race defects were artificially introduced to the bearing using electrical discharge machining [2]. The partial correlation integral algorithm is used to analyze the machine vibration data obtained throughout the life testing of a rolling element bearing [3]. A simple time series method for bearing fault feature extraction using singular spectrum analysis of the vibration signal is proposed [4].

A mathematical model for the ball bearing vibrations due to defect on the bearing race has been developed [5-6]. The effect of local defects on the nodal excitation functions is modelled. Simulated vibration signals are obtained [7-9]. Root mean square (RMS) values are obtained in the time domain and the high frequency resonance technique is used in the frequency domain [10-11]. Statistical properties of the vibration signals for healthy and defected structures are compared

[12-14]. Time domain analysis, frequency domain analysis and spike energy analysis have been employed to identify different defects in bearings [15]. The defect was detected using off the shelf portable vibration analysis hardware and software [16]. The detection of local defects existing on the races of deep groove ball bearing was investigated using envelope analysis and Duffing oscillator [17]. The resonance frequency in the first vibration mode of mechanical system was studied [18]. Finite element model can be effectively used to differentiate between vibration signatures for defects of different sizes in the bearing [19]. The vibrations generated by deep groove ball bearings having multiple defects on races were studied [20]. Wavelet transform provides a variable resolution time-frequency distribution from which periodic structural ringing due to repetitive force impulses were detected [21]. The discrete wavelet transform can be used as an effective tool for detecting single and multiple faults in the ball bearings [22]. Furthermore, discrete wavelet transform has been proposed for measuring outer race defect width of taper roller bearing. Experiments were carried out on a customized test setup [23].

Vibration signals from ball bearings having single and multiple defects on inner race, outer race, ball fault and combination of these faults have been considered for analysis [24]. The decomposed signal evidently splits the peak corresponding to the ball entry into and exit from the fault, enabling in an estimation of the defect size present in the bearing [25]. Wavelet packet analysis is a much better option than discrete wavelet transform. The method is designed in such a way that it can exploit the underlying physical concepts of the modulation

mechanism [26]. The experimental results indicate that, the wavelet packet analysis is a very reliable time-frequency domain approach capable of capturing high frequency transients in bearing signals [27]. Wavelet packet analysis is used as a powerful diagnostic method for the detection of initial bearing failures via stator current analysis [28]. The generated scalogram is used to identify and measure the seeded defects in bearing and gears [29]. The generated continuous wavelet transform coefficients are compared with the standard wavelet based scalogram. The scalogram generated from continuous wavelet transform is used to measure the duration that the roller takes to roll over the defect [30].

The aim of this study is to create a deep groove ball bearing model. Simulated vibration signals are obtained. The effect of the defects number on time and frequency domain parameters is investigated. The vibration monitoring methods are examined by using statistical parameters such as RMS, crest factor, kurtosis and skewness.

2. Experimental set-up

An experimental setup is employed to collect the vibration signals generated by incipient bearing defects. A schematic of test setup including the assembly and measurement equipments is shown in Fig. 1. The power unit of the testing rig is a three-phase asynchronous motor with variable speed up to 6000 rpm. The change of the shaft rotating direction and the adjustment of the shaft running speed can be achieved by means of a control unit which is mounted between the driving motor and the rotating shaft. An electronic wireless sensor is used for the measurement of the shaft speed. This arrangement is also equipped with an elastic claw coupling to damp out the high-frequency vibration generated by the motor.
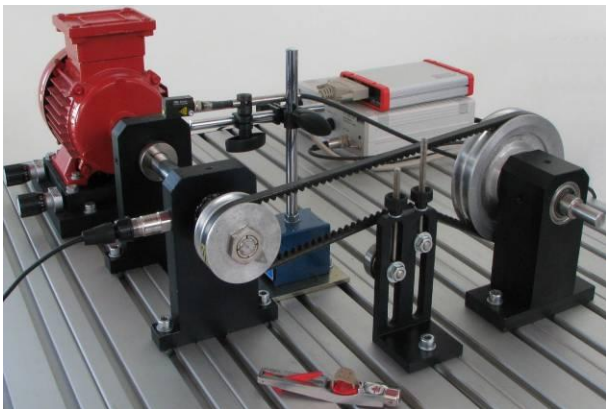

Fig. 1: Photograph of experimental test setup

3. Finite element model

A single row deep groove ball bearing SKF 6004 has been used in this study. The bearing geometry is shown in Fig. 2 and dimensions are given in Table 1. It is assumed that the contact between the outer surface of the outer ring and its mating surface on the casing structure is perfect meaning that no relative motion is permitted on the contact surface. The three-dimensional models of the housing and outer ring are modelled using ABAQUS. The housing model is created as per the

dimensions shown in Fig. 3. The bearing material is assumed as isotropic and linear-elastic with modulus of elasticity "E" of 203 GPa, Poisson's ratio "ν" of 0.29 and density "ρ" of 7850 kg/m^3. For the housing, the material is assumed to be isotropic and linear-elastic with modulus of elasticity "E" of 195 GPa, Poisson's ratio "ν" of 0.26 and density "ρ" of 7300 kg/m^3. The loads carried by the ball and roller bearings are transmitted through the rolling elements from one ring to the other [31].
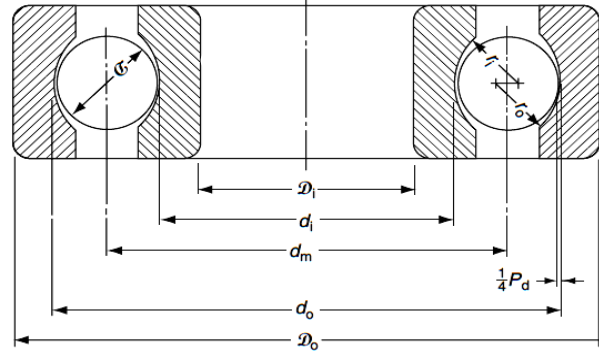

Fig. 2: Geometry of the deep groove ball bearing 6004 [31]

Table 1: Fluid and wind tunnel conditions

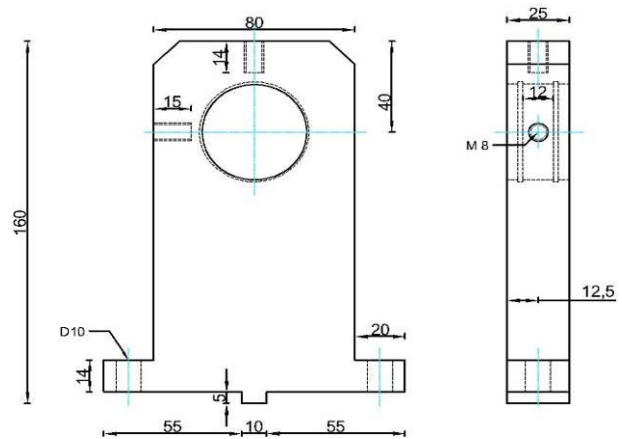| Dimension	Value
Outer diameter, D_o	42mm
Bore diameter, D_i	20mm
Pitch diameter, d_m	31mm
Raceway width, B	12mm
Ball diameter, D	6.35mm
Contact angle, α	0˚
Raceway diameter of outer race, d_o	34.8mm
Raceway diameter of inner race, d_i	27.2mm

Fig. 3: Dimensions (mm) of the housing structure

The relationship between load and deflection is:

$$Q = K\delta^n \tag{1}$$

where, "n" = 1.5 for ball bearings and "n" = 1.11 for roller bearings, "Q" is the ball or roller normal load, "δ" is deformation, and "K" is load-deflection factor. For a rigidly supported bearing subjected to a radial load, the radial deflection at any rolling element angular position is given by:

$$\delta_\psi = \delta_{max}\left[1 - \frac{1}{2\varepsilon}\left(1 - \cos\psi\right)\right] \tag{2}$$

$$\varepsilon = \frac{1}{2}\left(1 - \frac{P_d}{2\delta_r}\right) \qquad (3)$$

where, "δ_r" is the race radial shift, occurring at $\psi = 0^0$, "P_d" is the diametric clearance, "ε" is the load distribution factor. The angular extent of the load zone is determined by,

$$\psi_l = \cos^{-1}\frac{P_d}{2\delta_r} \qquad (4)$$

For ball bearings having zero clearance and subjected to a simple radial load determined that:

$$Q_\psi = Q_{max}\left[1 - \frac{1}{2\varepsilon}\left(1 - \cos\psi\right)\right]^n \qquad (5)$$

$$Q_{max} = \frac{4.37 F_r}{Z\cos\alpha} \qquad (6)$$

where, "F_r" is radial load and "Z" is number of balls. One of the simpler detection and diagnostic approaches is to analyze the measured vibration signal in the time domain. Whilst this can be as simple as visually looking at the vibration signal, other more sophisticated approaches can be used such as trending time domain statistical parameters. A number of statistical parameters can be defined as root mean square (RMS), crest factor, kurtosis, and skewness based upon the beta distribution.

$$RMS = \sqrt{\frac{1}{N}\sum_{i=1}^{N}\left[X(t) - \overline{X}\right]} \qquad (7)$$

$$Crest\ factor = \left[\max\cdot(X) - \min\cdot(X)\right]\big/RMS \qquad (8)$$

$$Kurtosis = \frac{1}{N}\sum_{i=1}^{N}\left[X(t) - \overline{X}\right]^4\bigg/RMS^4 \qquad (9)$$

$$Skewness = \frac{1}{N}\sum_{i=1}^{N}\left[X(t) - \overline{X}\right]^3\bigg/RMS^3 \qquad (10)$$

where $\overline{X}$ denotes the mean value of the discrete time signal X(t) having N data points. Time domain statistical parameters have been used as one-off and trend parameters in an attempt to detect the presence of incipient bearing damage. The ratio between the RMS of the defected bearing to that of the healthy one "R_{RMS}". The ratio between the crest factor parameter "CF" of the defected bearing to that of the healthy one "C_{CF}". The ratio between the kurtosis parameter "K" of the defected bearing to that of the healthy one "K_K". The ratio between skewness parameter "S" of the defected bearing to that of the healthy one "S_S".

The vibration data are calculated for vertical and horizontal directions for a broad range of rotational speed ranging from 1500 to 3500 rpm. The magnitude and the duration of the impulse force are related with the radial load carried by the outer race defect and the velocity of the rolling elements. A local defect is modelled by amplifying the magnitudes of the radial forces defined for the nodes which are in the defected area. The amplification constant of 3.58 is chosen. The frequency due to defect on outer race is given by,

$$f_o = \frac{Zf_s}{2}\left(1 - \frac{D}{d_m}\cos\alpha\right) \qquad (11)$$

4. Validation between the experimental and simulation results

The boundary conditions of the simulation process have been chosen to satisfy an acceptable correlation between the experimental set up and the simulated model. Fig. 4 shows an experimental acceleration signal for a healthy bearing and a bearing with a defected outer race, while the corresponding signal; that obtained from the simulation process; is shown in Fig. 5. It is observed from Figs. 4(a) and 5(a) that the dynamic response of the healthy bearing is approximately similar for the experimental and theoretical cases. Furthermore, it is noticed for the case of bearing with defected outer race that, the experimental results in Fig. 4(b) confirm that of the defected bearing simulation in Fig. 5(b). The difference between the experimental and simulation signals may be due to the interval time (0.0001sec) used in the dynamic model. These results indicated that the proposed method of simulation can be used to produce vibration data for condition monitoring applications.
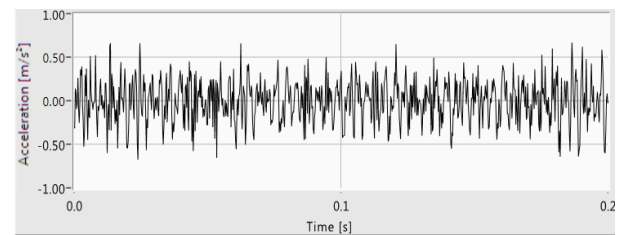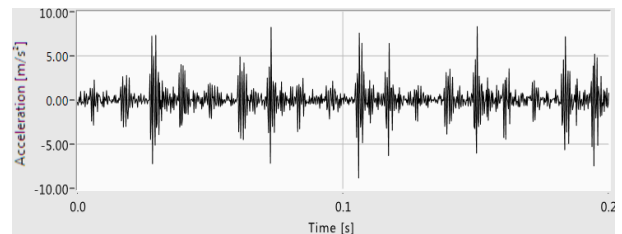

Fig. 4(a): Healthy bearing

Fig. 4(b): Bearing with defected outer race
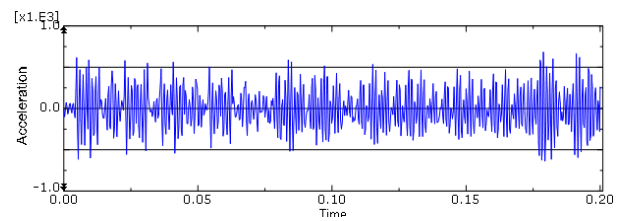
Fig. 4: Experimental acceleration signals for bearings
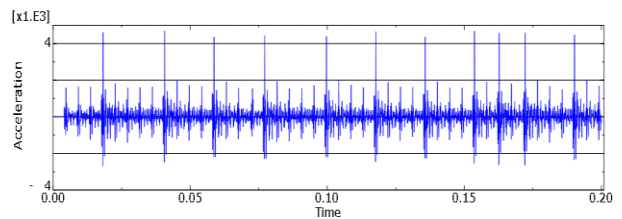

Fig. 5(a): Healthy bearing

Fig. 5(b): Bearing with defected outer race

Fig. 5: Acceleration response at horizontal point, 1500 rpm

Fig. 6 illustrates the RMS-ratio of the acceleration "R_{RMS}" for bearing with outer race defect versus the shaft speed. The RMS-ratio in the vertical direction displays

higher values than that of the horizontal direction. The value of the RMS-ratio decreases with the increase of the shaft speed. It is important to notice that, the higher values of the RMS-ratio on the vertical direction is connected to the position of the defect of the outer race, which means that the RMS-ratio increases at the position of the outer race defect. The analytical results describe the alteration of the bearing acceleration, velocity and displacement. Fig. 7 illustrates the variation of the RMS-ratio of the acceleration versus the shaft speed. The value of the RMS-ratio at point "P_1", i.e. in the vertical direction; is small in comparison to the horizontal one. Also, the RMS-ratio decreases with the increase of the shaft speed. Therefore, it is easier to detect the bearing defect at low speeds than that by high speeds which can be due to the reduction of the pulse interval. The comparison between the simulation and experiment results shows a good agreement between the results. However, the variation between the experimental and the simulation values may be due to the inequality of the defect size in both cases.
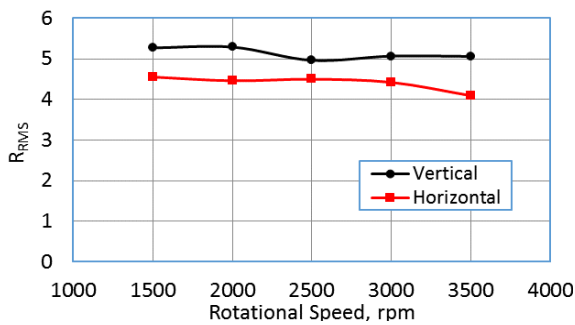
Fig. 6: Experimental variation of the acceleration RMS-ratio vs. Shaft speed for bearing with outer race defect
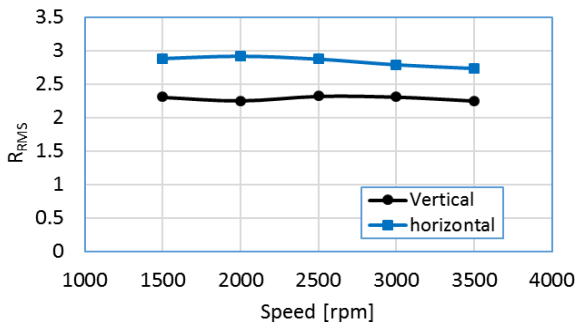
Fig. 7: Analytical variation of the acceleration RMS-ratio vs. Shaft speed for bearing model with outer race defect

5. Effect of defect number on the outer race

The number of defects on the outer race is increased step by step to show the effect of the defect number on time and frequency domain parameters. Multiple defects are introduced on the outer race. Firstly, single defect located at 0° and two defects located at 0° and 67.5° are analyzed. Then the number of defect increased to three and the locations of the local defects are 0°, 67.5° and 225°. Finally four defects are located on the outer race at the angular positions 0°, 67.5°, 225° and 270° as shown in Fig. 8. The RMS-ratio of the acceleration "R_{RMS}" for the case of multiple defects on the outer race at point "P_1", i.e. in the vertical direction and point "P2", i.e. in the horizontal direction are displayed in Figs 9 and 10

respectively. It can be seen that the RMS-ratio for four defects case gave high values at relatively low speeds. The same observation is valid for the vertical and horizontal directions.
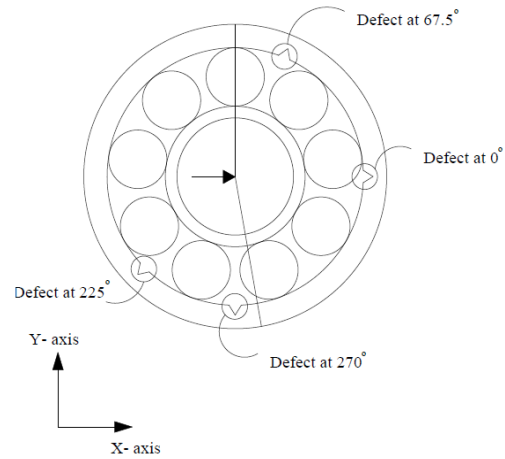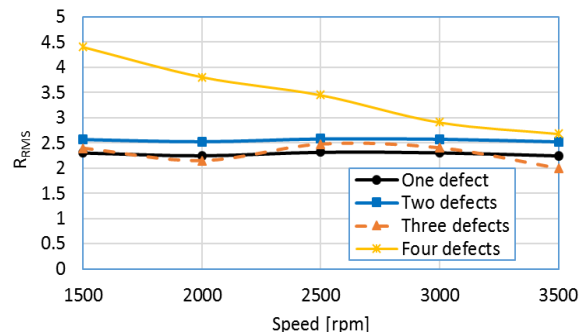

Fig. 8: Multiple defects on outer race

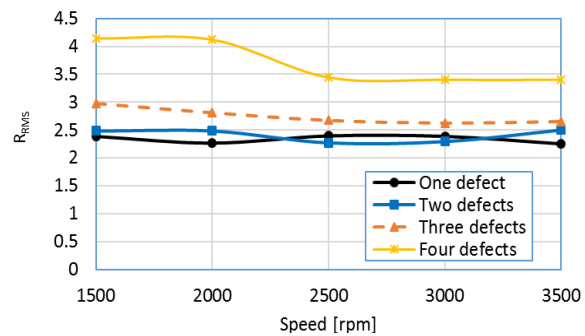Fig. 9: Acceleration RMS-ratio of multiple defects at point "P_1"

Fig. 10: Acceleration RMS-ratio of multiple defects at point "P_2"

It can observed from Fig. 11(a) that the crest factor ratio for acceleration "C_{CF}" of the one defect and two defects cases have no effect while the three defect and four defects cases show a greater effect. Fig. 11(b) illustrates the kurtosis ratio of the acceleration "K_K" at point "P_1". It can be observed that the kurtosis ratio is very small for all speeds except 1500 rpm with the three defects and four defects cases. It can be concluded that the multiple defects are difficult to monitor by using the kurtosis ratios for acceleration at point "P_1". It can be seen from Fig. 11(c) that the skewness ratio for acceleration "S_S" gave high values at four defects case. It can be concluded that the skewness ratio for acceleration "S_S" increases due to the increases in the number of defects. It can be noticed from Fig. 12(a) and Fig. 12(b) that the ratio between the time domain parameters of the defected and healthy bearings is very small for all speeds

by using the crest factor and kurtosis results. It can be concluded that the point "P_2" is not suitable during defect detection for the crest factor and kurtosis ratios. The three defects case gave high result at the point "P_2", for skewness ratio as shown in Fig. 12(c).
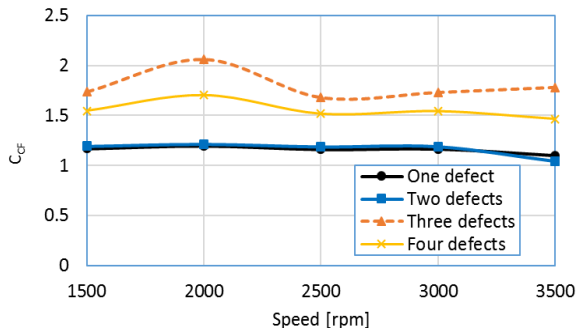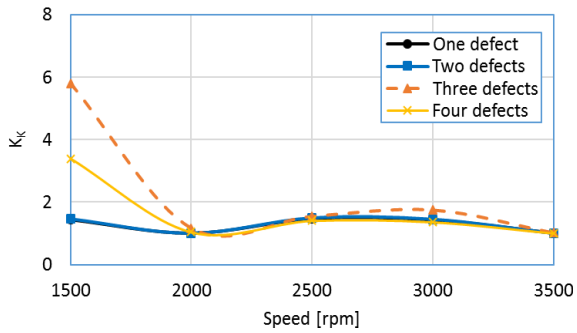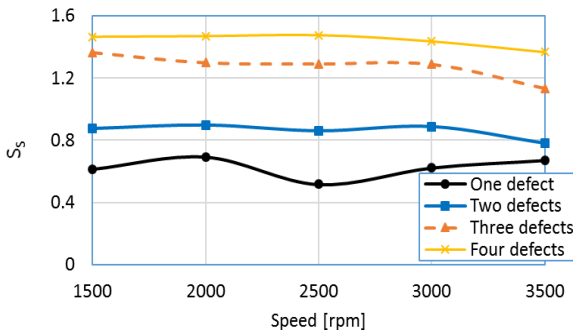
Fig. 11(a): Crest factor

Fig. 11(b): Kurtosis

Fig. 11(c): Skewness

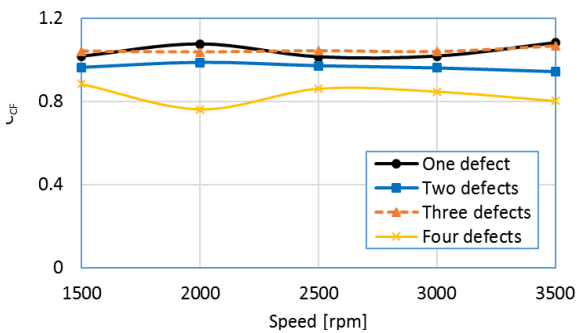**Fig. 11: Acceleration ratios of multiple defects at point "P_1"**
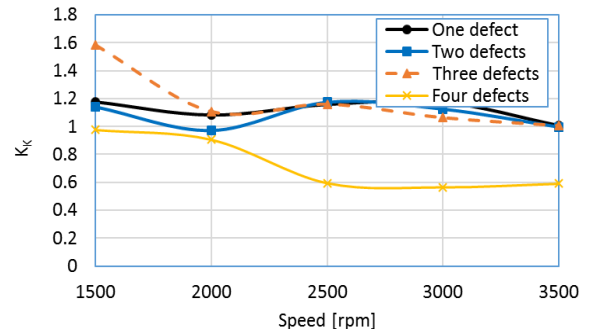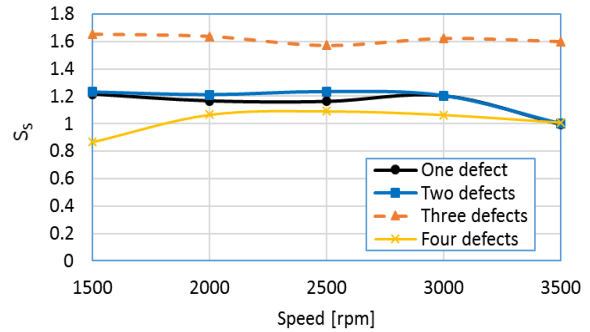
Fig. 12(a): Crest factor

Fig. 12(b): Kurtosis

Fig. 12(c): Skewness

Fig. 12: Acceleration ratios of multiple defects at point "P_2"

The RMS-ratio of the displacement "R_{RMS}" at point "P_1" is shown in Fig. 13. It can be noticed that the RMS-ratio gave high values and at relatively low speeds for the four defects case. The three defects and two defects cases have the same results at all speeds especially between 1500 rpm and 2500 rpm. Fig. 14 illustrates the RMS-ratio of the displacement "R_{RMS}" at point "P_2". It can be seen that the four defects case gave high values while the three defects case gave low values. It can be seen from Fig. 15(a) and Fig. 15(b) that the crest factor and kurtosis ratios at point "P_1" are very small for all speeds. It can be concluded that the defects detection is difficult by using the crest factor and kurtosis ratios. It can be observed from Fig. 15(c) that the skewness ratio "S_S" is very small for all speeds except 3500 rpm. Fig. 16(a) illustrates the crest factor ratio of the displacement at point "P_2". It can be concluded that the multiple defects gave no effect for all speeds except 3000 rpm. The same observation is valid at vertical and horizontal directions for the kurtosis and skewness ratios.
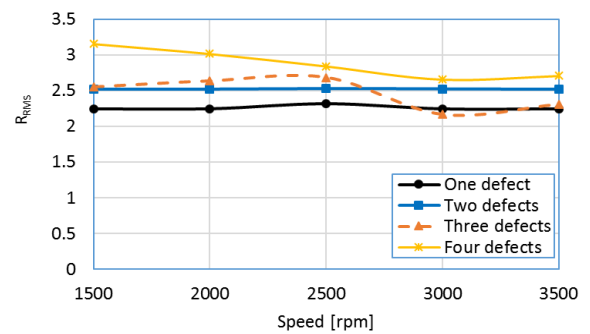
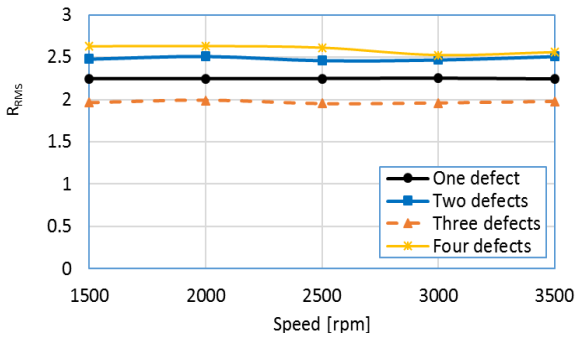**Fig. 13: Displacement RMS-ratio of multiple defects at point "P_1"**

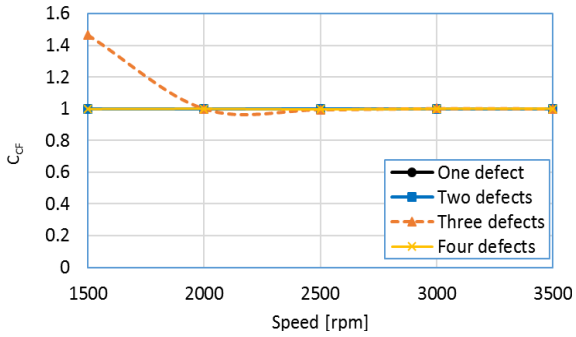**Fig. 14: Displacement RMS-ratio of multiple defects at point "P$_2$"**
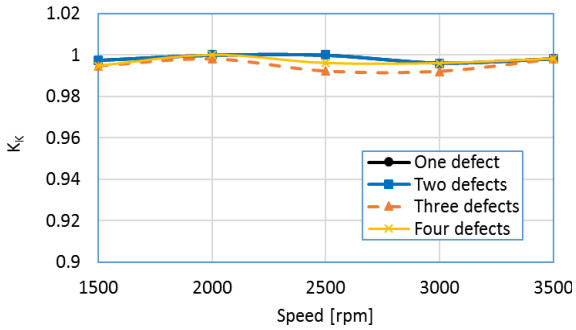

Fig. 15(a): Crest factor

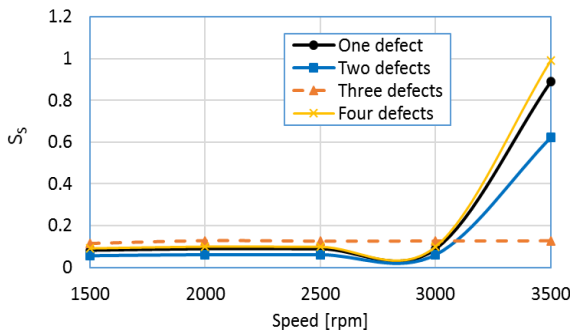**Fig. 15(b): Kurtosis**

Fig. 15(c): Skewness

Fig. 15: Displacement ratios of multiple defects at point "P$_1$"
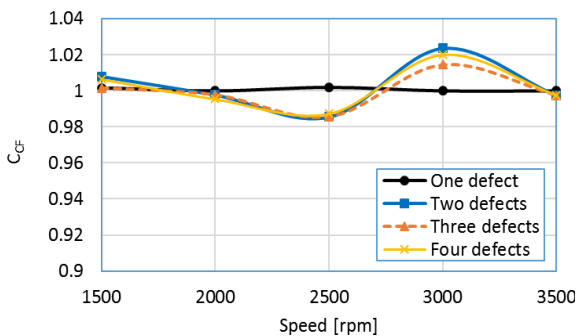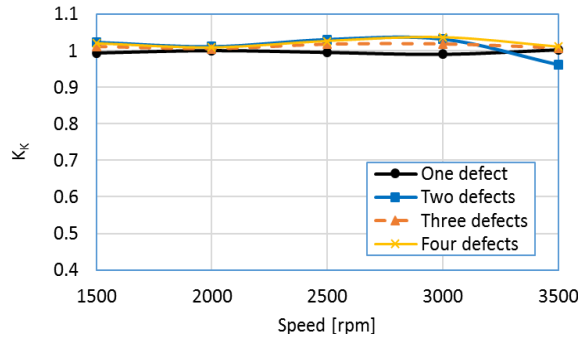

Fig. 16(a): Crest factor
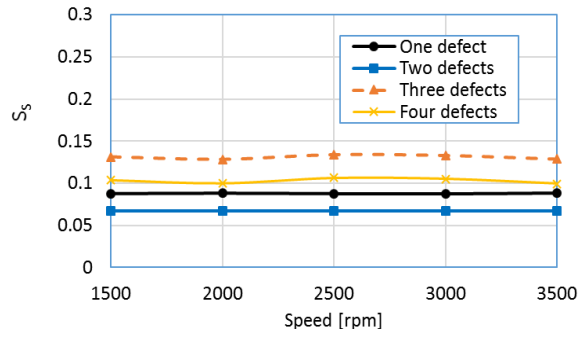

Fig. 16(b): Kurtosis

Fig. 16(c): Skewness

Fig. 16 Displacement ratios of multiple defects at point "P$_2$"

The RMS-ratio of the velocity "R$_{RMS}$" at point "P$_1$" is shown in Fig. 17. The same observation is valid for displacement, and velocity responses for the RMS-ratio while the three defects case gave low values. Fig. 18 illustrates the RMS-ratio of the velocity "R$_{RMS}$" at point "P$_1$". It can be observed that the four defects case give high values at all speeds except at 3000 rpm and 3500 rpm. It can observed from Fig. 18(a) that the crest factor of the velocity "C$_{CF}$" at point "P$_1$" is very small for all speeds and it is difficult to detect a defect. It can be noticed that the same observation is valid for the crest factor ratio at the point "P$_1$"and point "P$_2$". The same observation is valid for the kurtosis and crest factor ratios. It can be observed from Fig. 19(c) that the skewness ratio "S$_S$" is very small for all speeds at vertical direction. It can be concluded that the skewness ratios for the all defects cases gave very low results due to increase of speeds. Furthermore, it can be noticed from Fig. 20(c) that the skewness ratio "S$_S$" is very small for all speeds at point "P$_2$" except 2000 rpm & 3500 rpm.
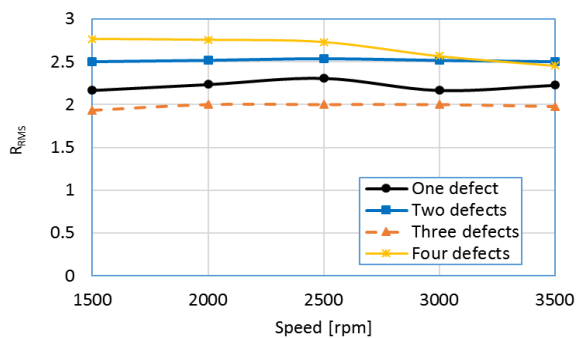

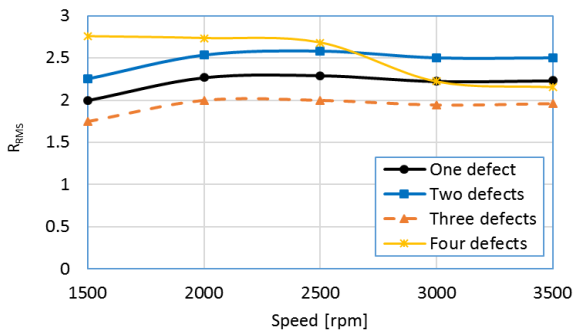**Fig. 17: Velocity RMS-ratio of multiple defects at point "P$_1$"**

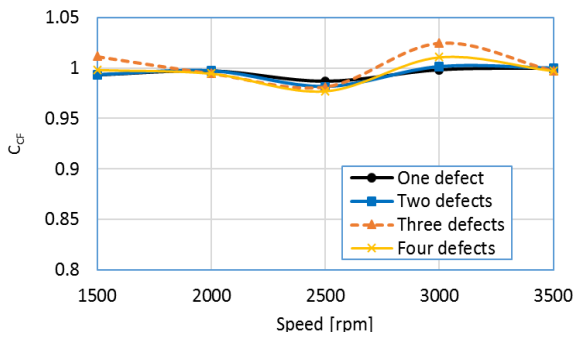**Fig. 18: Velocity RMS-ratio of multiple defects at point "P$_2$"**
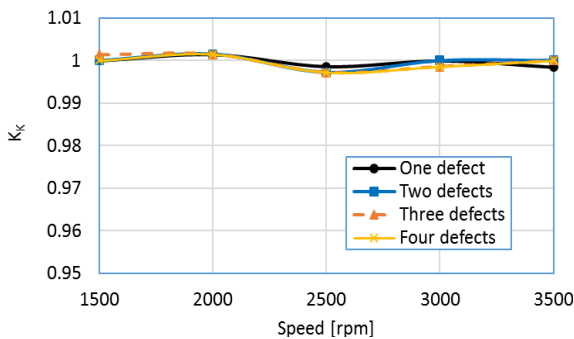

Fig. 19(a): Crest factor

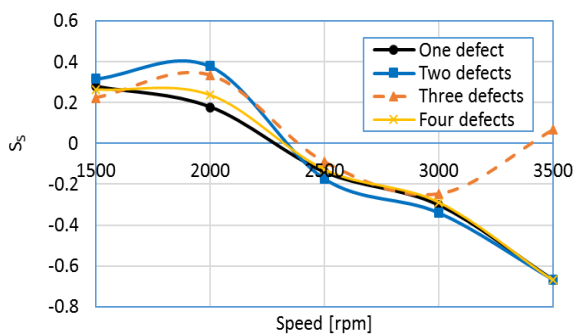**Fig. 19(b): Kurtosis**

Fig. 19(c): Skewness

Fig. 19: Velocity ratios of multiple defects at point "P$_1$"
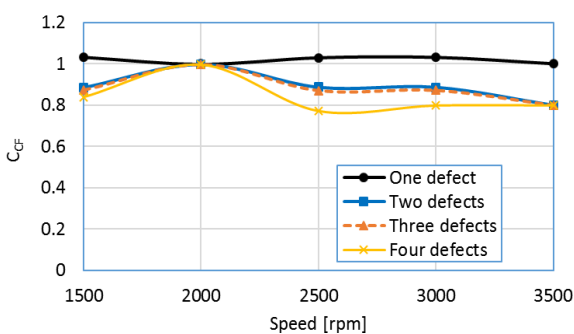

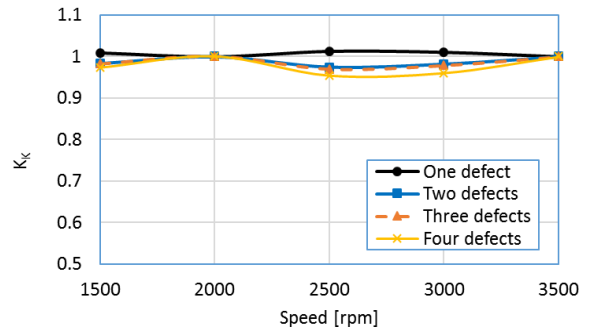**Fig. 20(a): Crest factor**

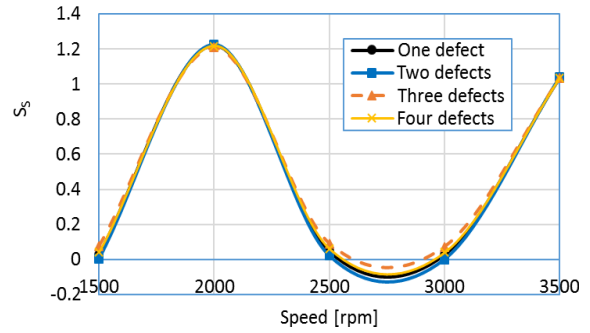**Fig. 20(b): Kurtosis**

Fig. 20(c): Skewness

Fig. 20: Velocity ratios of multiple defects at point "P$_2$"

6. Conclusions

In this paper, time domain statistical parameters extracted from simulation through dynamic models of gearbox ball bearing were used to detect the number of defects on the outer race of the bearing. The simulated data were also used to validate the performance of the experimental results. The statistical parameters ratio between of the defected and healthy bearings increase due to the increases in the number of defect on the outer race of the bearing. The multiple defects are difficult to monitor by using the crest factor, kurtosis and skewness ratios for displacement and velocity responses.

REFERENCES:

[1] Y.T. Sheen. 2004. A complex filter for vibration signal demodulation in bearing defect diagnosis, *J. Sound and Vibration*, 276, 105-119. http://dx.doi.org/10.1016/j.jsv. 2003.08.007.

[2] H. Ocak and K.A. Loparo. 2004. Estimation of the running speed and bearing defect frequencies of an induction motor from vibration data, *Mechanical Systems and Signal Processing*, 18, 515-533. http://dx.doi.org/10. 1016/S0888-3270(03)00052-9.

[3] S. Janjarasjitta, H. Ocak and K.A. Loparo. 2008. Bearing condition diagnosis and prognosis using applied nonlinear dynamical analysis of machine vibration signal, *J. Sound and Vibration*, 317, 112-126. http://dx.doi.org/ 10.1016/j.jsv.2008.02.051.

[4] B. Muruganatham, M.A. Sanjith, B. Krishnakumar and S.A.V. Satya Murtyk. 2013. Roller element bearing fault diagnosis using singular spectrum analysis, *Mechanical Systems and Signal Processing*, 35, 150-166. http://dx. doi.org/10.1016/j.ymssp.2012.08.019.

[5] M.S. Patil, J. Mathew, P.K. Rajendrakumar and S. Desai. 2011. A theoretical mode to predict the effect of localized defect on vibrations associated with ball

bearing, *Int. J. Mechanical Sciences*, 52, 1193-1201. http://dx.doi.org/10.1016/j.ijmecsci.2010.05.005.

[6] A. Rafsanjania, S. Abbasion, A. Farshidianfar and H. Moeenfard. 2009. Nonlinear dynamic modeling of surface defect sin rolling element bearing systems, *J. Sound and Vibration*, 319, 1150-1174. http://dx.doi.org/ 10.1016/j.jsv.2008.06.043.

[7] Z. Kiral. 2002. *Simulation and Analysis of Vibration Signals Generated by Rolling Element Bearings with Defects*, PhD Thesis, The University of Izmir, Turkey.

[8] J. Liu, Y. Shao and T.C. Lim. 2012. Vibration analyses of ball bearings with a localized defect applying piecewise response function, *Mechanism and Machine Theory*, 56, 156-169. http://dx.doi.org/10.1016/j. mechmachtheory.2012.05.008.

[9] H. Cao, L. Niu and Z. He. 2012. Method for vibration response simulation and sensor placement optimization of a machine tool spindle system with a bearing defect, *Sensors*, 12, 8732-8754. http://dx.doi.org/10.3390/s1207 08732.

[10] P. Kadarno and Z. Taha. 2008. Vibration Analysis of Defected Ball Bearing using Finite Element Model Simulation, *Proc. 9th Asia Pasific Industrial Engg. & Management Systems Conf.*.

[11] Z. Taha and N.T. Dung. 2010. Rolling element bearing fault detection with a single point defect on the outer raceway using FEA, *Proc. 11th Asia Pacific Industrial Engg. & Management Systems Conf.*.

[12] Z. Kiral and H. Karagulle. 2003. Simulation and analysis of vibration signals generated by rolling element bearing with defects, *Tribology Int.*, 36, 667-678. http://dx.doi. org/10.1016/S0301-679X(03)00010-0.

[13] T. Karacay and N. Akturk. 2009. Experimental diagnostics of ball bearings using statistical and spectral methods, *Tribology Int.*, 42, 836-843. http://dx.doi.org/ 10.1016/j.triboint.2008.11.003.

[14] Y.H. Kim, A.C.C. Tan, J. Mathew and B.S. Yang. 2006. Condition monitoring of low speed bearings: A comparative study of the ultrasound technique versus vibration measurements, *Proc. WCEAM*.

[15] M. Amarnath, R. Shrinidhi, A Ramachandra and S.B. Kandagal. 2004. Prediction of defects in antifriction bearings using vibration signal analysis, *IE (I) J.-MC*.

[16] M.S. Johnson Jr. 2000. Vibration tests for bearing wear, *ASHRAE J.*.

[17] V.N. Patel, N. Tandon and R.K. Pandey. 2012. Defect detection in deep groove ball bearing in presence of external vibration using envelope analysis and duffing oscillator, *Measurement*, 45, 960-970. http://dx.doi.org/ 10.1016/j.measurement.2012.01.047.

[18] Y.T. Sheen. 2010. An envelope analysis based on the resonance modes of the mechanical system for the bearing defect diagnosis, *Measurement*, 43, 912-934. http://dx.doi.org/10.1016/j.measurement.2010.03.011.

[19] U.A. Patel and S. Rajkamal. 2012. Vibrational analysis of self align ball bearing having a local defect through FEA and its validation through experiment, *Int. J. Modern Engg. Research*, 2, 1073-1080.

[20] V.N. Patel, N. Tandon and R.K. Pandey. 2014. Vibrations generated by rolling element bearings having multiple local defects on races, *Procedia Technology*, 14, 312-319. http://dx.doi.org/10.1016/j.protcy.2014.08.041.

[21] C.J. Li and J. Ma. 1997. Wavelet decomposition of vibrations for detection of bearing-localized defects, *NDT & E Int.*, 30, 143-149. http://dx.doi.org/10.1016/S0963-8695(96)00052-7.

[22] S. Prabhakar, A.R. Mohanty and A.S Sekhar. 2002. Application of discrete wavelet transform for detection of ball bearing race faults, *Tribology Int.*, 35, 793-800. http://dx.doi.org/10.1016/S0301-679X(02)00063-4.

[23] R. Kumar and M. Singh. 2013. Outer race defect width measurement in taper roller bearing using discrete wavelet transform of vibration signal, *Measurement*, 46, 537-545. http://dx.doi.org/10.1016/j.measurement. 2012.08.012.

[24] V. Purushotham, S. Narayanan and S.A.N. Prasad. 2005. Multi-fault diagnosis of rolling bearing elements using wavelet analysis and hidden Markov model based fault recognition, *NDT & E Int.*, 38, 654-664. http://dx.doi.org /10.1016/j.ndteint.2005.04.003.

[25] S. Khanam, N. Tandon and J.K. Dutt. 2014. Fault size estimation in the outer race of ball bearing using discrete wavelet transform of the vibration signal, *Proc. Tech.*, 14, 12-19. http://dx.doi.org/10.1016/j.protcy.2014. 08.003.

[26] N.G. Nikolaou and I.A. Antoniadis. 2002. Rolling element bearing fault diagnosis using wavelet packets, *NDT & E Int.*, 35, 197-205. http://dx.doi.org/10.1016/ S0963-8695(01)00044-5.

[27] Y. Li. 2006. *Online Condition Monitoring of Rolling Element Bearings*, MSc Thesis, The University of Waterloo, Canada.

[28] J. Zarei and J. Poshtan. 2007. Bearing fault detection using wavelet packet transform of induction motor stator current, *Tribology Int.*, 40, 763-769. http://dx.doi.org/10. 1016/j.triboint.2006.07.002

[29] D.P. Jena and S.N. Panigrahi. 2012. Bearing and gear fault diagnosis using adaptive wavelet transform of vibration signals, *Proc. Engg.*, 50, 265-274.

[30] D.P. Jena and S.N. Panigrahi. 2014. Precise measurement of defect width in tapered roller bearing using vibration signal, *Measurement*, 55, 39-50. http://dx.doi.org/10. 1016/j.measurement.2014.04.023.

[31] T.A. Harris and M.N. Kotzalas. 2006. *Essential Concepts of Bearing Technology*, 5th Edition, Taylor & Francis.